

SUPERNOVA REMNANT CROSSING A DENSITY JUMP: A THIN SHELL MODEL

Yang Chen^{1,2}, Fan Zhang¹, Rosa M. Williams², and Q. Daniel Wang²

ABSTRACT

The environments of supernova explosion are often inhomogeneous and there may be jumps in their density structure. We have developed a semi-analytic model under the thin-shell approximation for supernova remnants that evolve crossing a density jump in the ambient medium. The generic evolutionary relations are presented for the blast wave after impacting on a cavity wall, which may be produced by the energetic stellar wind from the supernova progenitor. The relations can also be extended to the case that the blast waves break out from a dense cloud if different density contrast is used. This model is applied to N132D, a well-known cavity-born supernova remnant whose evolution has not yet been quantitatively estimated in a cavity scenario due to lack of model formulae, and self-consistent physical parameters are obtained.

Subject headings: ISM: bubbles — ISM: kinematics and dynamics — shock waves — supernova remnants — supernova remnants: individual: N132D

1. Introduction

The environments of supernova explosion are often inhomogeneous and there may be jumps in their density structure. A massive star can excavate a low density cavity with its energetic stellar wind and ionizing radiation in the circumstellar space before it explodes. It is also possible that supernova may explode in a dense cloud and subsequently break out from the cloud into a low density region. These supernova remnants (SNRs) cannot be simply treated with the canonical evolutionary laws such as the Sedov relation (Sedov 1959). In the former case, a blast wave collides with a cavity wall after it expands effortlessly into the cavity. A similar situation has been suggested to have occurred in various supernova remnants such as N132D (Hughes 1987). In the latter case, the blast wave propagates at a

¹Department of Astronomy, Nanjing University, Nanjing 210093, P.R.China

²Department of Astronomy, B619E-LGRT, University of Massachusetts, Amherst, MA01003

higher velocity after it breaks out of the cloud, as is suggested for 3C 391 (Reynolds & Moffett 1993). It would be of interest to develop an analytic model showing how the evolution of such kind of supernova remnants deviates from the canonical solution.

In a study of SNR evolution in a dense molecular cloud, Wheeler et al. (1980) briefly discussed the effect of a pre-SN cavity, suggesting that the remnant will evolve rapidly into the radiative phase after it encounters the cavity wall. Chevalier and Liang (1989) presented a self-similar model for both the structure of the shocked powerlaw ejecta and the shock propagation into the circumstellar shell. However, the ejecta structure becomes unimportant when the mass swept up by the blast wave significantly exceeds the mass of the ejecta. Investigation of supernova blast waves crossing a density jump has been carried out by hydrodynamic simulation. Tenorio-Tagle et al. (1990, 1991) made numerical simulations of the supernova shock interacting with a wind-driven shell (see also a review by Franco et al. 1991 and references therein). Tenorio-Tagle, Bodenheimer, & Yorke (1985) have also presented a numerical simulation of the evolution of a remnant resulting from supernova explosions in or near molecular clouds.

An analytical model would not only complement the numerical simulation, but would allow for exploring a large parameter space and more directly provide physical insights into the evolution of this sort of SNRs. It has been shown by many authors (e.g., McCray 1987, Blinnikov, Imshennik, & Utrobin 1982, and others) that a thin-shell model (Kompaneets 1960), though approximate, is convenient and valid in revealing the general evolution of the supernova blast wave. The approach was applied in a numerical algorithm to calculate the evolution of SNRs in a density gradient (see Wang et al. 1992). This method has also been applied analytically to other explosive events, e.g., a cosmic ray blast wave (Morfill & Drury 1981). Therefore we use the same approach to obtain an analytic/semi-analytic approximation to seek the basic evolutionary rule of the blast wave after an impact on a cavity wall or a breakout from a cloud.

2. Thin-shell Model of Impact on a Wall

For the ambient environment of supernova, we assume a density structure of medium $\rho = \rho_i = 1.4n_i m_{\text{H}}$ for $r < r_j$ and $\rho = \rho_0 = 1.4n_0 m_{\text{H}}$ for $r \geq r_j$ (where n_i and n_0 are the number densities of H atoms inside and outside the density jump, respectively). In this scenario, the ejecta or blast wave is assumed to expand easily until it hits upon the cavity wall at r_j . By the time the ejecta or blast wave arrives at r_j , the SNR could be in the Sedov phase or even still in the free expansion phase, depending on the parameters r_j and ρ_i . Denote the density ratio by $\beta \equiv (\rho_i + \bar{\rho}_{\text{ej}})/\rho_0$, where $\bar{\rho}_{\text{ej}}$ is the average density of the ejecta mass over the cavity

within r_j , so here we discuss the case $\beta < 1$. The swept-up material is assumed to be in a thin shell and the mass in a conical section of solid angle $\Delta\Omega$ is given by

$$\Delta M_s = \frac{1}{3}\Delta\Omega\rho_0 [r_s^3 - r_j^3(1 - \beta)]. \quad (1)$$

On the assumption that most of the explosion energy is thermalized by the time when the blastwave impacts the wall or soon after that, the thermal pressure in a spherical remnant is given by

$$p = \frac{(\gamma - 1)E}{4\pi r_s^3/3} = \frac{E}{2\pi r_s^3}, \quad (2)$$

where E is the total energy and the adiabatic index $\gamma = 5/3$. The momentum equation for the conical section is

$$\frac{d}{dt}(\Delta M_s v_s) = p r_s^2 \Delta\Omega, \quad (3)$$

From the equations (1), (2), and (3), we have

$$r_s \frac{d}{dt} \left[(r_s^3 - r_j^3(1 - \beta)) \frac{dr_s}{dt} \right] = \frac{3E}{2\pi\rho_0}. \quad (4)$$

2.1. Adiabatic phase

Before the radiative phase, the supernova remnant is assumed to be adiabatic and the energy to remain unchanged: $E \approx E_0$. Then eq.(4) has a solution

$$v_s^2 = \left(\frac{dr_s}{dt} \right)^2 = \left(\frac{E_0}{\pi\rho_0} \right) \frac{r_s^3 - 3r_j^3(1 - \beta) \ln r_s + C}{[r_s^3 - r_j^3(1 - \beta)]^2}, \quad (5)$$

where integral constant C must be determined according to the initial condition at $r_s = r_j$. The problem can be divided into two cases presented below.

In the first case, the supernova remnant has already been in the Sedov phase by the time t_j when $r_s = r_j$. The Sedov evolution law under the thin shell approximation is given by $r_s = (\xi E_0/\rho_i)^{1/5} t^{2/5}$ where $\xi = 25/4\pi$ (e.g. McCray 1987), so the initial velocity at r_j is $v_s^2 = E_0/(\pi\rho_i r_j^3)$. The blast wave velocity is thus

$$\frac{dr_s}{dt} = \sqrt{\frac{E_0}{\pi\rho_0} \frac{\sqrt{r_s^3 - r_j^3(1 - \beta)[1 - 3 \ln(r_j/r_s)]}}{r_s^3 - r_j^3(1 - \beta)}} \quad (6)$$

namely

$$v_s = \left(\frac{E_0}{\pi\rho_0 r_s^3} \right)^{1/2} F_v^{(A)}(\lambda_j), \quad (7)$$

where $\lambda_j \equiv r_j/r_s$ and

$$F_v^{(A)}(\lambda_j) \equiv \frac{\sqrt{1 - \lambda_j^3(1 - \beta)(1 - 3 \ln \lambda_j)}}{1 - \lambda_j^3(1 - \beta)}. \quad (8)$$

In the second case, the remnant is still in the free expansion stage when arriving at r_j . In this case, $\rho_i < \bar{\rho}_{ej}$; and, for simplicity, $\beta \approx 0$ is assumed. For $\beta = 0$, the above initial condition cannot be used, and instead, the convergence of eq.(5) at $r_s = r_j$ is entailed, so $C = -r_j^3 + 3r_j^3 \ln r_j$. Thus, interestingly, the velocity is still described by eqs.(6)–(8) (but with $\beta = 0$).

Eq.(6) gives rise to

$$t - t_j = \sqrt{\frac{\pi \rho_0}{E_0}} \int_{r_j}^{r_s} \frac{r^3 - r_j^3(1 - \beta)}{\sqrt{r^3 - r_j^3(1 - \beta)[1 - 3 \ln(r_j/r)]}} dr \quad (9)$$

or

$$[F_r^{(A)}(\lambda_j)]^{2/5} r_s = \left(\frac{E_0}{\pi \rho_0}\right)^{1/5} (t - t_j)^{2/5}, \quad (10)$$

where

$$F_r^{(A)}(\lambda_j) \equiv \int_{\lambda_j}^1 \frac{\lambda^3 - \lambda_j^3(1 - \beta)}{\sqrt{\lambda^3 - \lambda_j^3(1 - \beta)[1 - 3 \ln(\lambda_j/\lambda)]}} d\lambda = \int_{\lambda_j}^1 \frac{\lambda^{3/2}}{F_v^{(A)}(\lambda_j/\lambda)} d\lambda \quad (11)$$

with $\lambda = r/r_s$. The above integration (at $r_j \neq 0$) can only be performed numerically, as plotted in Fig.1.

Note that, for the special case $r_j = \lambda_j = t_j = 0$, $F_v^{(A)} = 1$ and $F_r^{(A)} = 2/5$, so we immediately come from eq.(10) back to the Sedov solution $r_s = (\xi E_0/\rho_0)^{1/5} t^{2/5}$ where $\xi = 25/4\pi$ under the thin-shell approximation (e.g. McCray 1987).

As shown in Fig.1, both functions $F_v^{(A)}(\lambda_j)$ and $F_r^{(A)}(\lambda_j)$ vary with parameter β . For $\beta \neq 0$, function $F_v^{(A)}(\lambda_j)$ starts from $\beta^{-1/2}$, as a limit value found for eq.(8) at $\lambda_j = 1$ or $r_s = r_j$. The remnant is decelerated rapidly after it enters the cavity wall, as indicated by the ensuing rapid decrease of $F_v^{(A)}(\lambda_j)$. Just when r_s surpasses r_j , the smaller β is, the more drastically $F_v^{(A)}$ drops and the more quickly $F_v^{(A)}$ approaches the asymptotic curve for $\beta = 0$. In addition, these asymptotic values are of order unity, implying a crude factor of velocity decrease $\sim \beta^{-1/2}$ or a ram pressure (ρv_s^2) roughly recovered to that before the impact (see eq.[7]).

In the limit case $\beta = 0$, immediately after the remnant strikes the cavity wall [$1 - \lambda_j \equiv (r_s - r_j)/r_s \ll 1$], the behavior of $F_v^{(A)}$ can be described by the Taylor series

$$F_v^{(A)}(\lambda_j) \simeq \frac{1}{\sqrt{2}} \left[1 + \frac{1}{2}(1 - \lambda_j) \right], \quad (12)$$

and the shock velocity at $r_s = r_j$ (i.e. $\lambda_j = 1$) is

$$v_s(r_j) = \left(\frac{E_0}{2\pi\rho_0 r_j^3} \right)^{1/2} = 1.4 \times 10^3 \left(\frac{E_0}{10^{51} \text{ ergs}} \right)^{1/2} \left(\frac{n_0}{1 \text{ cm}^{-3}} \right)^{-1/2} \left(\frac{r_j}{5 \text{ pc}} \right)^{-3/2} \text{ km s}^{-1}, \quad (13)$$

a factor $\sqrt{2}$ lower than the velocity $v_s = (E_0/\pi\rho_0 r_j^3)^{1/2}$ the shock would otherwise have in the Sedov solution. Still in the case $\beta = 0$, the linear relation [eq.(12)] is found to be a good approximation of $F_v^{(A)}$ for $1 \geq \lambda_j \gtrsim 0.2$ (see Fig.1).

At the other extremity $\lambda_j \ll 1$, $F_v^{(A)}(\lambda_j)$ approaches to 1 according to

$$F_v^{(A)}(\lambda_j) \simeq 1 + \frac{1}{2}(1 - \beta)(1 + 3 \ln \lambda_j)\lambda_j^3, \quad (14)$$

which allows for any values of β .

The numerical solution of function $F_r^{(A)}(\lambda_j)$ in eq.(11) shows that it starts from 0 at $\lambda_j = 1$ and approaches the other extremity $\lambda_j = 0$ in similar trends for various values of β (Fig.1). For $1 - \lambda_j \ll 1$, in the case $\beta \neq 0$, its behavior can be approximated by a series:

$$F_r^{(A)}(\lambda_j) \approx \frac{1}{10\sqrt{\beta}} \left[(-9 + 13\beta) + 50(1 - \beta)\lambda_j - 105(1 - \beta)\lambda_j^2 + 4(16 - 17\beta)\lambda_j^{5/2} \right], \quad (15)$$

which is obtained by expanding function $F_v^{(A)}(\lambda_j/\lambda)$ in eq.(11) to the second order of the small quantity $(1 - \lambda_j/\lambda)$; in the case $\beta = 0$, however,

$$F_r^{(A)}(\lambda_j) \approx \frac{1}{6\sqrt{2}} \left(3 + 2\lambda_j + 3\lambda_j^2 - 8\lambda_j^{5/2} \right). \quad (16)$$

This series expansion is found valid in a broad range $1 \geq \lambda_j \gtrsim 0.3$ (Fig.1).

At the extremity $\lambda_j \ll 1$, function $F_r^{(A)}(\lambda_j)$ converges to 0.4 conforming to

$$F_r^{(A)}(\lambda_j) \approx \frac{2}{5} \left(1 - \lambda_j^{5/2} \right) + 5(1 - \beta) \left(\lambda_j^{5/2} - \lambda_j^3 \right) + 3(1 - \beta)\lambda_j^3 \ln \lambda_j, \quad (17)$$

which is valid for any value of β .

For $\beta \gtrsim 0.1$, numerical integration (Fig.1) shows that $F_r^{(A)}(\lambda_j)$ as a whole does not vary significantly with various β . If we take $\beta = 1$ for simplicity, it corresponds to the uniform case; eq.(8) yields $F_v^{(A)} = 1$ and eq.(11) yields

$$F_r^{(A)}(\lambda_j) = \frac{2}{5}(1 - \lambda_j^{5/2}) \quad (18)$$

(see the long dashed line in Fig.1). If this expression is adopted as a *crude* approximation of $F_r^{(A)}(\lambda_j)$ for $\beta \gtrsim 0.1$, eq.(10) then gives a Sedov-like evolution

$$t - t_j \approx \sqrt{\frac{\rho_0}{\xi E_0}} \left(r_s^{5/2} - r_j^{5/2} \right), \quad (19)$$

where $\xi = 25/4\pi$ but can be replaced with the canonical value 2.026.

The adiabatic phase will come to an end when the gas temperature drops to $T_c = 6 \times 10^5$ K (Blinnikov et al. 1982). With the relation $kT_s = (3/16)\mu m_H v_s^2$ (where the mean atomic weight $\mu = 0.61$), Eq.(7) with $\rho_0 = 1.4n_0 m_H$ gives the location r_c of the phase transition:

$$\frac{r_c^3}{[F_v^{(A)}(r_j/r_c)]^2} = (4.7 \text{ pc})^3 \left(\frac{E_0}{10^{51} \text{ ergs}} \right) \left(\frac{n_0}{10^2 \text{ cm}^{-3}} \right)^{-1} \quad (20)$$

If $\beta \ll 1$, the linear approximation (12) is adopted and the above formula is simplified as

$$r_c^2 r_j \approx (3.8 \text{ pc})^3 E_{51} (n_0/10^2 \text{ cm}^{-3})^{-1} \quad (21)$$

where $E_{51} = E_0/(10^{51} \text{ ergs})$. For $\beta \ll 1$, the sudden deceleration of the remnant on impacting the cavity wall makes it possible that the shocked gas temperature $T_s(r_j)$ has already gotten below T_c and the radiative phase has begun before the velocity falls on the asymptotic curve (for $\beta \rightarrow 0$, see Fig.1). In this case, the adiabatic phase lasts so little time after the impact that it essentially may be ignored. Therefore it is possible that a previously freely expanding remnant directly enters the radiative phase after it strikes the wall and the adiabatic phase is abortive if $r_j \gtrsim 3.8 \text{ pc } E_{51}^{1/3} (n_0/10^2 \text{ cm}^{-3})^{-1/3}$.

2.2. Radiative phase

When the shell is cooled down by radiation, it is assumed to be driven by the thermal pressure of the still hot gas interior to the shell. The internal hot gas suffers from the energy loss by the expansion:

$$\frac{dE}{dt} = -4\pi r_s^2 v_s p. \quad (22)$$

Eq.(22), inserted with eq.(2), yields

$$E = E_0 (r_c/r)^2. \quad (23)$$

Now, eq.(4) becomes

$$r_s^3 \frac{d}{dt} \left[(r_s^3 - r_j^3(1 - \beta)) \frac{dr_s}{dt} \right] = \frac{3E_0 r_c^2}{2\pi\rho_0}, \quad (24)$$

with a solution

$$\frac{dr_s}{dt} = \sqrt{\frac{3E_0 r_c^2}{\pi\rho_0} \frac{\sqrt{(r_s - r_c) + r_j^3(r_s^{-2} - r_c^{-2})(1 - \beta)/2 + [r_c - (r_j^3/r_c^2)(1 - \beta)(1 - 3 \ln(r_j/r_c))]}{r_s^3 - r_j^3(1 - \beta)}}}. \quad (25)$$

In this solution, we have used eq.(6) as the initial condition of the shock velocity at the phase transition point $r_s = r_c$ and $t = t_c$.

Setting $\lambda_c \equiv r_c/r_s$, $\eta \equiv r_c/r_j$, and $\mu = (1 - \beta)/\eta^3$, eq.(25) is rewritten as

$$v_s = \left(\frac{3E_0 r_c^2}{\pi \rho_0 r_s^5} \right)^{1/2} F_v^{(R)}(\lambda_c), \quad (26)$$

where

$$F_v^{(R)}(\lambda_c) \equiv \frac{\sqrt{(1 - \lambda_c) + (\mu/2)\lambda_c(\lambda_c^2 - 1) + (\lambda_c/3)[1 - \mu(1 + 3 \ln \eta)]}}{1 - \mu\lambda_c^3}. \quad (27)$$

Eq.(25) gives

$$t - t_c = \sqrt{\frac{\pi \rho_0}{3E_0 r_c^2}} \times \int_{r_c}^{r_s} \frac{r^3 - r_j^3(1 - \beta)}{\sqrt{(r - r_c) + r_j^3(r^{-2} - r_c^{-2})(1 - \beta)/2 + [r_c - (r_j^3/r_c^2)(1 - \beta)(1 - 3 \ln(r_j/r_c))]} / 3} dr \quad (28)$$

or

$$[F_r^{(R)}(\lambda_c)]^{2/7} r_s = \left(\frac{3E_0 r_c^2}{\pi \rho_0} \right)^{1/7} (t - t_c)^{2/7}, \quad (29)$$

where

$$\begin{aligned} F_r^{(R)}(\lambda_c) &\equiv \int_{\lambda_c}^1 \frac{\lambda^3 - \mu\lambda_c^3}{\sqrt{(\lambda - \lambda_c) + (\mu/2)\lambda_c(\lambda_c^2/\lambda^2 - 1) + (\lambda_c/3)[1 - \mu(1 + 3 \ln \eta)]}} d\lambda \\ &= \int_{\lambda_c}^1 \frac{\lambda^{5/2}}{F_v^{(R)}(\lambda_c/\lambda)} d\lambda. \end{aligned} \quad (30)$$

The numerical values of functions $F_v^{(R)}(\lambda_c)$ and $F_r^{(R)}(\lambda_c)$ are plotted in Figs.(2)–(4), where it is seen that both functions depend on the parameters β and η . For most cases of (η, β) combination, $F_v^{(R)}(\lambda_c)$ starts from $[1 - \mu(1 + 3 \ln \eta)]^{1/2}/[\sqrt{3}(1 - \mu)]$ at $\lambda_c = 1$ (i.e. $r_s = r_c$); but for $(\eta, \beta) = (1, 0)$, it starts from $6^{-1/2}$ and the Taylor series

$$F_v^{(R)}(\lambda_c) \simeq \frac{1}{\sqrt{6}} \left[1 + \frac{5}{6}(1 - \lambda_c) + \frac{35}{72}(1 - \lambda_c)^2 \right] \quad (\text{for } 1 - \lambda_c \ll 1) \quad (31)$$

can acts as a good approximation in the range $1 > \lambda_c \gtrsim 0.5$ (Fig.2). In the latter case, when the radiative phase begins at $r_s = r_c = r_j$ ($\lambda_j = \lambda_c = 1$), eq.(26) turns back to eq.(13). For any (η, β) combination, $F_v^{(R)}(\lambda_c)$ approaches 1 at the other end, $\lambda_c = 0$, according to

$$F_v^{(R)}(\lambda_c) \simeq 1 - \frac{1}{12}[4 + \mu(5 + 6 \ln \eta)]\lambda_c. \quad (32)$$

It is noted that, at the limit $\lambda_c \rightarrow 0$ (or $r_s \gg r_c$), one has $F_v^{(R)} = 1$ and $F_r^{(R)} = 2/7$, and then eq.(29) is identical to the canonical solution for SNRs in radiative phase: $r_s = (147E_0r_c^2/4\pi\rho_0)^{1/7}t^{2/7}$ (e.g. McCray 1987; Blinnikov et al. 1982).

While we could not find an analytic integration for eq.(30), we seek for a series approximation for $\lambda_c \ll 1$:

$$F_r^{(R)}(\lambda_c) \approx \frac{1}{5040} \left\{ 1440 + 168\lambda_c(4 + 5\mu) + 35\lambda_c^2(4 + 5\mu)^2 - \lambda_c^{7/2}(2672 + 2240\mu + 875\mu^2) \right. \\ \left. - 84\lambda_c\mu \left[-12 - 5\lambda_c(4 + 5\mu) + \lambda_c^{5/2}(32 + 25\mu) \right] \ln \eta - 1260\lambda_c^2(-1 + \lambda_c^{3/2})\mu^2 \ln^2 \eta \right\} \quad (33)$$

Eq.(33) is obtained by expanding the integrand in eq.(30) to the second order of small quantity λ_c/λ and, for the case $\eta \gtrsim 1.1$, is found to be very close to the numerical values in the entire range (see Figs.3 and 4). In the case $\eta = 1$ and $\beta \neq 0$, similarly we get a series approximation for $1 - \lambda_c \ll 1$:

$$F_r^{(R)}(\lambda_c) \approx \frac{1}{70} \sqrt{\frac{3}{\beta}} \left[\beta (135 - 434\lambda_c + 455\lambda_c^2 - 156\lambda_c^{7/2}) + 7 (-15 + 54\lambda_c - 55\lambda_c^2 + 16\lambda_c^{7/2}) \right], \quad (34)$$

and in the case $(\eta, \beta) = (1, 0)$ ($1 - \lambda_c \ll 1$),

$$F_r^{(R)}(\lambda_c) \approx \frac{\sqrt{6}}{252} (27 + 42\lambda_c + 35\lambda_c^2) - \frac{26}{21} \sqrt{\frac{2}{3}} \lambda_c^{7/2}. \quad (35)$$

Eq.(35) is a very good approximation for $(\eta, \beta) = (1, 0)$ in the range $1 \geq \lambda_c \gtrsim 0.3$ (Fig.2).

3. Thin-shell Model of Breakout of a Cloud

We assume a configuration of environment density similar to that in the former case, except that $\rho_i > \rho_0$ or $\beta > 1$. The material in the cloud is dense enough that we can assume the supernova remnant has been in the adiabatic (Sedov) phase by the time of breakout. Moreover, because the density ρ_0 outside the cloud is so low, we need not consider the radiative phase in this scenario, as it is unlikely the SNR would yet have entered this phase. Therefore most of the evolutionary solutions for the adiabatic phase established in the former case are compatible with this case, given a replacement of $\beta > 1$. Functions $F_v^{(A)}(\lambda_j)$ and $F_r^{(A)}(\lambda_j)$ for $\beta > 1$ are plotted in Fig.5.

4. Applications

4.1. Applicability

The model developed above can, strictly speaking, only be applied to an SNR of spherical symmetry. In reality, an SNR is usually not symmetric, which could be caused by the motion of the progenitor for instance. While a good fraction of stars show a considerable proper motion, there are still objects with a low proper motion. In practice, as long as the asymmetry is reasonably small, our model should still provide a useful approximation. As a general condition, the dynamical response (characterized by a sound traveling timescale) due to the non-spherical symmetry of the density jump surface should not be rapid enough compared with the blastwave propagation after crossing the jump surface.

Furthermore, we have assumed that the density jump happens only once. However, this may not be true for an SNR evolving in a stellar wind bubble, for example. In this case, a dense shell, surrounding a low density bubble, may be approximated as two density jumps. In principle, such multiple density jumps can be incorporated into an analytic approach. But this is a bit too complicated to be included in the present work. Here, we concentrate on exploring the effect of one density jump on the evolution of an SNR, which is still evolving in the shell. This particular situation is important, because of the expected strong density jump effect on the X-ray emission of the SNRs.

In the range of applicability discussed here, the solutions derived in section 2 can conveniently be used in estimating the parameters of relevant supernova remnants. For example, X-ray observations provide the X-ray luminosity or the volume emission measure of the X-ray emitting gas as well as the gas temperature that is related to the velocity of the blast wave. Note that the temperature measured in a plasma model fit to the overall spectrum of an SNR only represents a characteristic mean temperature of the shocked gas, even for the Sedov blast wave. In principle, one can derive a relation between this mean temperature and the shock velocity. This problem may also be resolved to some degree with the spatially resolved spectroscopic data, which allow for the extraction of the spectrum of the freshly-shocked gas. By use of eq.(7) (or eq.[26]) and eq.(10) (or eq.[29]) together with a relation between the volume emission measure and the density of the ambient medium, any three among the five parameters, the density n_0 , explosion energy E , the age of the remnant t , the density contrast β , and the fractional radius of the density jump λ_j , can be derived from the other two, given the three known parameters, the radius remnant r_s , the shell velocity v_s , and the volume emission measure EM . According to this recipe, we apply the model developed above to SNR N132D that are conjectured to have expanded from a stellar wind cavity into a region of dense medium and derive relevant physical parameters.

4.2. SNR N132D

N132D, an SNR in the Large Magellanic Cloud, lies near the northern boundary of an associated molecular cloud (Banas et al. 1997). The inconsistency between the kinematic age and the Sedov dynamical age led to the suggestion that the supernova explosion occurred in a low-density cavity evacuated by the stellar wind and ionizing radiation of a high-mass progenitor (Hughes 1987; Morse et al. 1996; Hughes, Hayashi, & Koyama 1998). Morse et al. (1995) derived a kinematic age of 3150 ± 200 yr from the measurements of the velocities of fast moving oxygen-rich filaments. Morse et al. (1996) studied the optical photoionization precursor based on the [OIII] λ 5007 surface brightness and derive a preshock density of $n_0 \sim 3 \text{ cm}^{-3}$ and a blast shock velocity $v_s \sim 800 \text{ km s}^{-1}$. They find that these results would be trapped in unreconcilable contradictions (either the inferred explosion energy is unusually high ($\gtrsim 10^{52}$ ergs), or the inferred age is much larger than the kinematic age), unless the blast wave has been traveling much faster in the past, probably by expanding into a low density cavity. However, quantitative estimates of the evolution of the SNR expanding from the cavity into the cavity wall have not yet been carried out because of lack of proper evolutionary formulae.

N132D is an oxygen-rich SNR but no evidence was found by the *Hubble Space Telescope* (*HST*) for the presence oxygen-burning products. This fact was taken by Blair et al. (2000) to suggest a Wolf-Rayet (WR) star which ended at a Type Ib SN explosion. However, X-ray data from *XMM-Newton* (Behar et al. 2001; Aschenbach 2002) do show the presence of significant proportions of Si and Fe. If these elements are actually present in the ejecta, rather than the surrounding ISM, this might tend to contradict the scenario of a Type Ib explosion. Earlier X-ray findings by Hwang et al. (1993) using the Focal Plane Crystal Spectrometer on *Einstein* also found strong Fe lines, which the authors used to support the scenario of a massive progenitor (with masses over $20M_\odot$ favored). Therefore we assume that the core collapse SN explosion occurred in a stellar wind cavity blown by a massive progenitor, possibly a WR star.

The recent *XMM-Newton* X-ray observation of N132D shows a clear shell feature from which most of the ion emission lines arise and a centrally confined Fe K emission characteristic of a high temperature component (Behar et al. 2001; Aschenbach 2002). According to the *ASCA* data analysis (Hughes et al. 1998), the high X-ray luminosity ($\sim 3 \times 10^{37} \text{ ergs s}^{-1}$) of the shell comes from the shock interaction with the dense material at the cavity wall, with an X-ray spectral normalization factor $N_s \sim 5 \times 10^{12} \text{ cm}^{-5}$, and hence a volume emission measure $EM = 4\pi d^2 N_s \sim 1.5 \times 10^{60} \text{ cm}^{-3}$ (where $d \approx 50 \text{ kpc}$) (Hughes et al. 1998). The *ASCA* spectral fit gives a temperature for the X-ray emitting gas $kT_X \sim 0.7 \text{ keV}$. Recently the *XMM* RGS spectrum indicates a low temperature component of $\sim 0.6 \text{ keV}$ (Aschenbach

2002), and the *XMM* EPIC-PN spectrum indicates ~ 0.9 keV (Behar et al. 2001). Compared with the central high temperature Fe K emission, the low temperature component could basically ascribed to the shell gas. If 0.7 keV is taken as a mean value of the postshock temperature, it corresponds to a shell velocity $v_s \sim 770$ km s $^{-1}$, consistent with the above value derived from the optical observation.

We consider a scenario in which the blast wave propagates rapidly in the wind cavity until it encounters the cavity wall, where it is slowed down drastically. Assuming the swept-up cavity material has been compressed sufficiently, the volume emission measure, under the thin-shell approximation, is given by

$$EM \approx \frac{(4n_0)^2}{3} \pi r_s^3 [1 - \lambda_j^3(1 - \beta)], \quad (36)$$

where the radius of the remnant r_s is about 12 pc. For various values of β and λ_j , we get from EM the estimates of the density at the cavity wall, n_0 , and hence the swept-up gas mass, $M_s = 100M_\odot M_2$ (eq.[1]), as plotted in Fig.6 together with other physical parameters obtained from the following calculations. With the aid of eq.(8) for function $F_v^{(A)}(\lambda_j)$, we then get from eq.(7) an estimate of the explosion energy E_0 . The age of the remnant, $t = 10^3 t_3$ yr, consists of two parts, t_j (Sedov evolution before the blast wave reaches the cavity wall) and $t - t_j$ (duration after the impact). The latter is obtained from eq.(10) with eq.(15) for function $F_r^{(A)}(\lambda_j)$.

It can be found from Fig.6 that the kinematic age $t \sim 3 \times 10^3$ yr and the preshock density $n_0 \sim 3$ cm $^{-3}$ can be reproduced by means of the wind cavity model, if parameters

$$\beta \sim 0.1 \quad \text{and} \quad \lambda_j \sim 0.94-0.95$$

are adopted. With this set of parameters, we also have $E_{51} \sim 3$ and thus avoid an unreasonably high inference. As a comparison, if β is adopted lower, E_{51} would be too high; and if λ_j is larger, t would be too large compared with the kinematic age. If n_0 is fixed at 3 cm $^{-3}$, the EM (eq.[36]) entails a density contrast $\beta < 0.2$. We note that, the previous overestimates of E_0 corresponds to the case that $F_v^{(A)}(\lambda_j)$ is taken as 1 in eq.(7); in order for E_0 to be of normal value, $F_v^{(A)}(\lambda_j)$ has to be > 1 . This condition for $F_v^{(A)}$ is satisfied around our best-fit parameters $\beta \sim 0.1$ and $\lambda_j \sim 0.94-0.95$ (see Fig.1), which implies that the blast wave is still in the course of abrupt deceleration within the wind-blown shell.

With the best-fit parameters, we also know that it takes the blast wave $t_j \sim 2.2 \times 10^3$ yr to travel in the cavity and that the velocity of the blast wave just before impacting the cavity wall is $v_j \sim 1.9 \times 10^3$ km s $^{-1}$ which is decreased to the present value ~ 800 km s $^{-1}$ over a duration of ~ 700 yr. Also with these quantities, it is easy to confirm a sufficient compression of the swept-up cavity material, consistent with the above EM approximation

(eq.[36]). Moreover, the total swept-up mass is $M_s \sim 170M_\odot$, to which the gas originally inside the cavity contributes $\sim 60M_\odot$. The latter mass seems too high for a wind cavity, however this is not a surprise, if a small part of gas are evaporated from the cavity wall or/and if interstellar clumps have been left within the cavity so that the cavity might contain a substantial amount of interstellar material. The existence of interstellar clumps is reasonable in view of the proximity of the remnant to the southern molecular cloud (Banas et al. 1997). In fact, a shocked interstellar cloudlet has been found in the remnant by the *HST* (Blair et al. 2000). In addition, the swept-up mass of the cavity gas ($\sim 60M_\odot$) suggests that the SNR has been in the Sedov phase by the time it collides with the cavity wall.

5. Conclusion

Using the thin-shell approximation, we have developed a semi-analytic model for supernova remnants which evolve crossing a density jump in the environmental medium. The generic evolutionary relations are found for two cases, impact of the blast wave on a cavity wall and breakout of the blast wave from a dense cloud. In the impact case, both the adiabatic and radiative phases are investigated; while in the breakout case, only the adiabatic phase is considered and the evolution relations are found to be an extension of those in the former case with different density contrast. In the impact case, it is also found that the remnant will evolve rapidly into the radiative phase and even the adiabatic phase could last so short that it seems to be abortive if the medium density at the cavity wall is sufficiently high. The developed model is applied to the cavity-born supernova remnant N132D whose evolution has not yet been quantitatively estimated in a cavity scenario due to lack of proper model formulae and self-consistent physical parameters are obtained.

We are grateful to Rino Bandiera for helpful advices during this work. An anonymous referee is thanked for critical comments which have helped appreciably improve the model application. John P. Hughes is also thanked for helpful comments. YC and FZ acknowledge support from NSFC grants 1007003 & 10221001 and grant NKBRSF-G19990754 of China Ministry of Science and Technology. This work is partially supported by NASA-grant SAO GO-12068X and NASA LTSA grant NAG5-7935.

REFERENCES

- Aschenbach, B. 2002, in Proceedings of the 270 WE-Heraeus Seminar on “Neutron Stars, Pulsars and Supernova Remnants”, eds. W.Becker, H.Lesch, & J.Trümper, MPE Report 278, pp. 13-25 (astro-ph/0208492)
- Banas, K.R., Hughes, J.P., Bronfman, L., & Nyman, L.-Å., 1997, ApJ, 480, 607
- Behar, E., Rasmussen, A.P., Griffiths, R.G., Dennerl, K., Audard, M., Aschenbach, B., & Brinkman, A.C. 2001, A&A, 365, L242
- Blair, W.P., Morse, J.A., Raymond, J.C., Kirshner, R.P., Hughes, J.P., Dopita, M.A., Sutherland, R.S., Long, K.S., Winkler, P.F. 2000, ApJ, 537, 667
- Blinnikov, S. I., Imshennik, V. S., & Utrobin, V. P. 1982, Sov. Astron. Lett., 8, 361
- Chevalier, R. A. & Liang, E. P. 1989, ApJ, 344, 332
- Franco, J., Tenorio-Tagle, G., Bodenheimer, P., & Różyczka, M. 1991, PASP, 103, 803
- Hughes, J. P. 1987, ApJ, 314, 103
- Hughes, J. P., Hayashi, I., & Koyama, K. 1998, ApJ, 505, 732
- Hwang, U., Hughes, J. P., Canizares, C.R., & Markert, T.H., 1993, ApJ, 414,219
- Kompaneets, A.S. 1960, Sov. Phys. Dokl., 5, 46
- McCray, R. 1987, in *Spectroscopy of astrophysical plasmas*, Ed. by Dalgarno, A. & Layzer, D.(Cambridge Univ. Press), p.256
- Morfill, G.E. & Drury, L.O’C. 1981, MNRAS, 197, 369
- Morse, J.A., Blair, W.P., Dopita, M.A., Hughes, J.P., Kirshner, R.P., Long, K.S., Raymond, J.C., Sutherland, R.S., & Winkler, P.F. 1996, AJ, 112, 509
- Morse, J.A., Winkler, P.F., & Kirshner, R.P. 1995, AJ, 109, 2104
- Reynolds, S.P., & Moffett, D.A. 1993, AJ, 105, 2226 in IAU #214 symposium
- Tenorio-Tagle, G., Bodenheimer, P., & Yorke, H.W. 1985, A&A, 145, 70
- Tenorio-Tagle, G., Bodenheimer, P., Franco, J., & Różyczka, M. 1990, MNRAS, 244, 563
- Tenorio-Tagle, G., Różyczka, M., Franco, J., & Bodenheimer, P. 1991, MNRAS, 251, 318

Wang, Z.-R., Qu, Q.-Y., Luo, D., McCray, R., & Mac Low, M.-M. 1992, ApJ, 388, 127

Wheeler, J. C., Mazurek, T. J., & Sivaramakrishnan, A. 1980, ApJ, 237, 781

Sedov, L.I. 1959, Similarity and Dimensional Methods in Mechanics (New York: Academic)

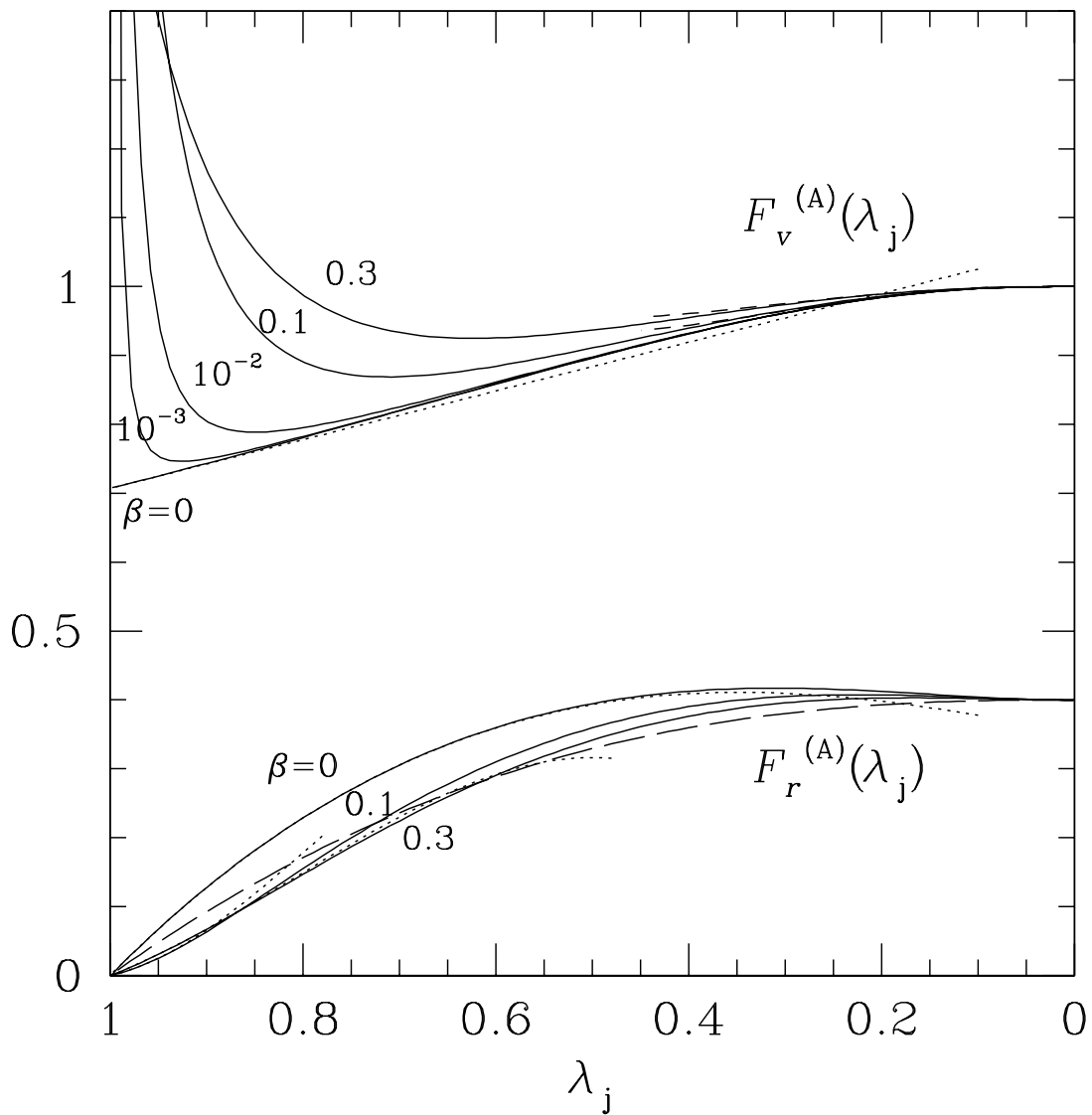


Fig. 1.— Plots of functions $F_v^{(A)}(\lambda_j)$ and $F_r^{(A)}(\lambda_j)$ for the impact model ($\beta < 1$). The solid lines denote the accurate values of eqs.(8) and (11). The four dotted lines, from upper to lower, stand for eq.(12) and eq.(16) in the limit case $\beta = 0$, and eq.(15) for $\beta = 0.1, 0.3$, respectively, while the two short dashed lines stand for eq.(14) in the cases $\beta = 0$ and $\beta = 0.3$. The long dashed line is the plot of eq.(18).

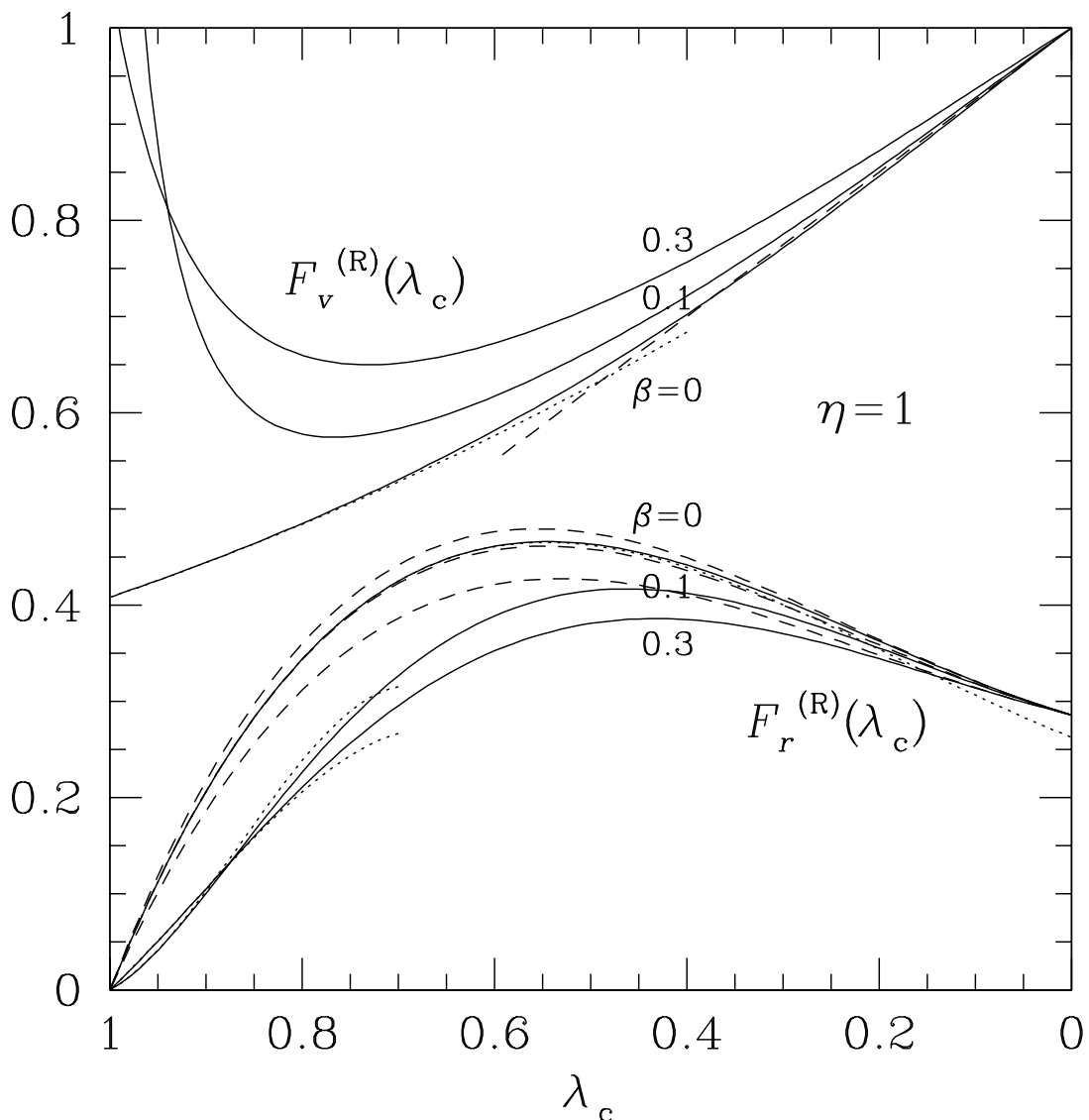


Fig. 2.— Plots of functions $F_v^{(R)}(\lambda_c)$ and $F_r^{(R)}(\lambda_c)$ for $\eta = 1$. The solid lines denote the accurate values of eqs.(27) and (30). The dotted lines stand for eqs.(31) and (35) in the case $\beta = 0$ and eq.(34) in the cases $\beta = 0.1, 0.3$, respectively. The dashed lines stand for eq.(32) for $\beta = 0$ and eq.(33) for $\beta = 0, 0.1, 0.3$, respectively.

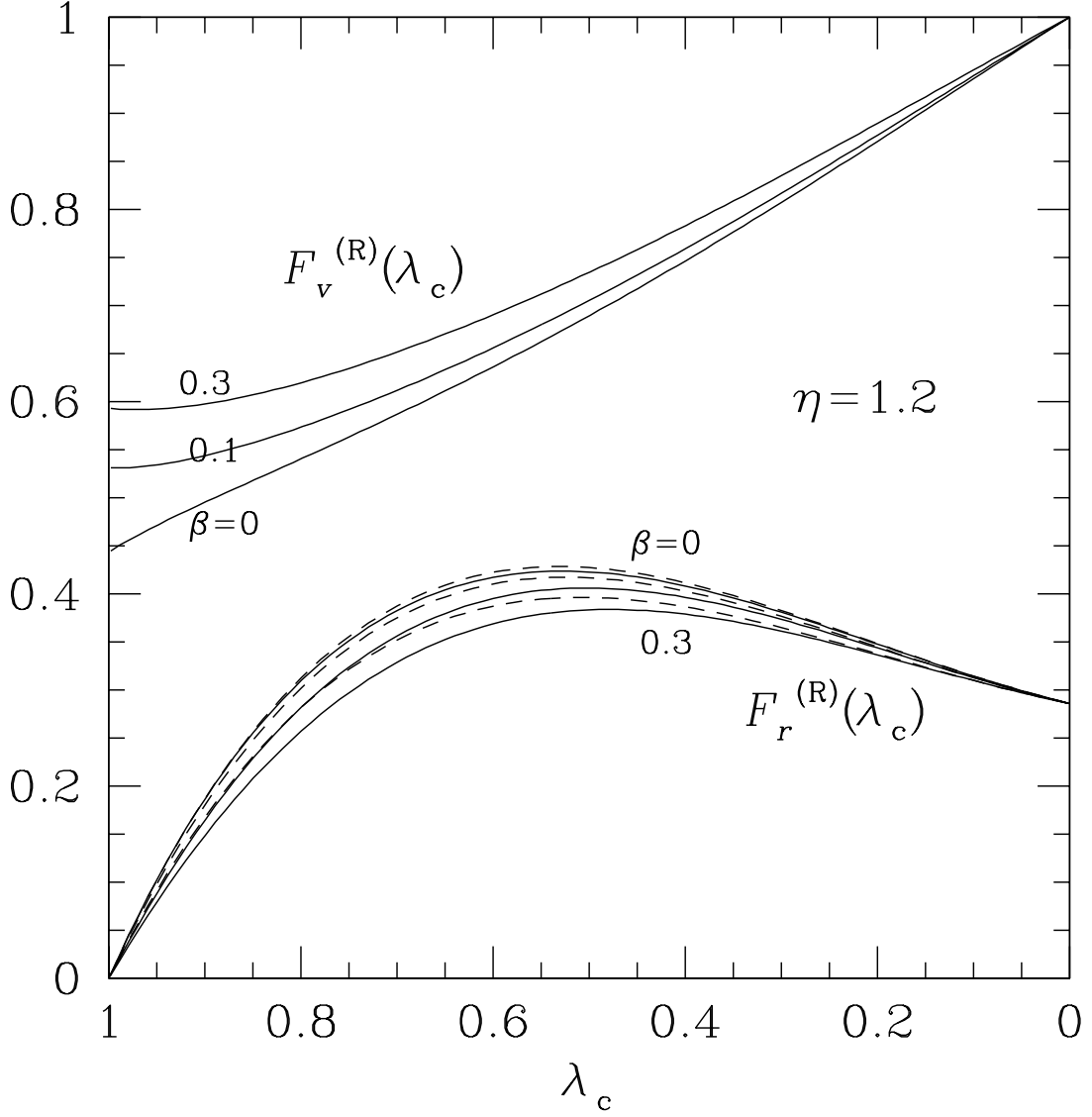


Fig. 3.— Plots of functions $F_v^{(R)}(\lambda_c)$ and $F_r^{(R)}(\lambda_c)$ for $\eta = 1.2$. The solid lines denote the accurate values of eqs.(27) and (30) and the dashed lines represent eq.(33). The solid and dashed curves of $F_r^{(R)}(\lambda_c)$ are plotted for $\beta = 0, 0.1$, and 0.3 , respectively, from upper to lower.

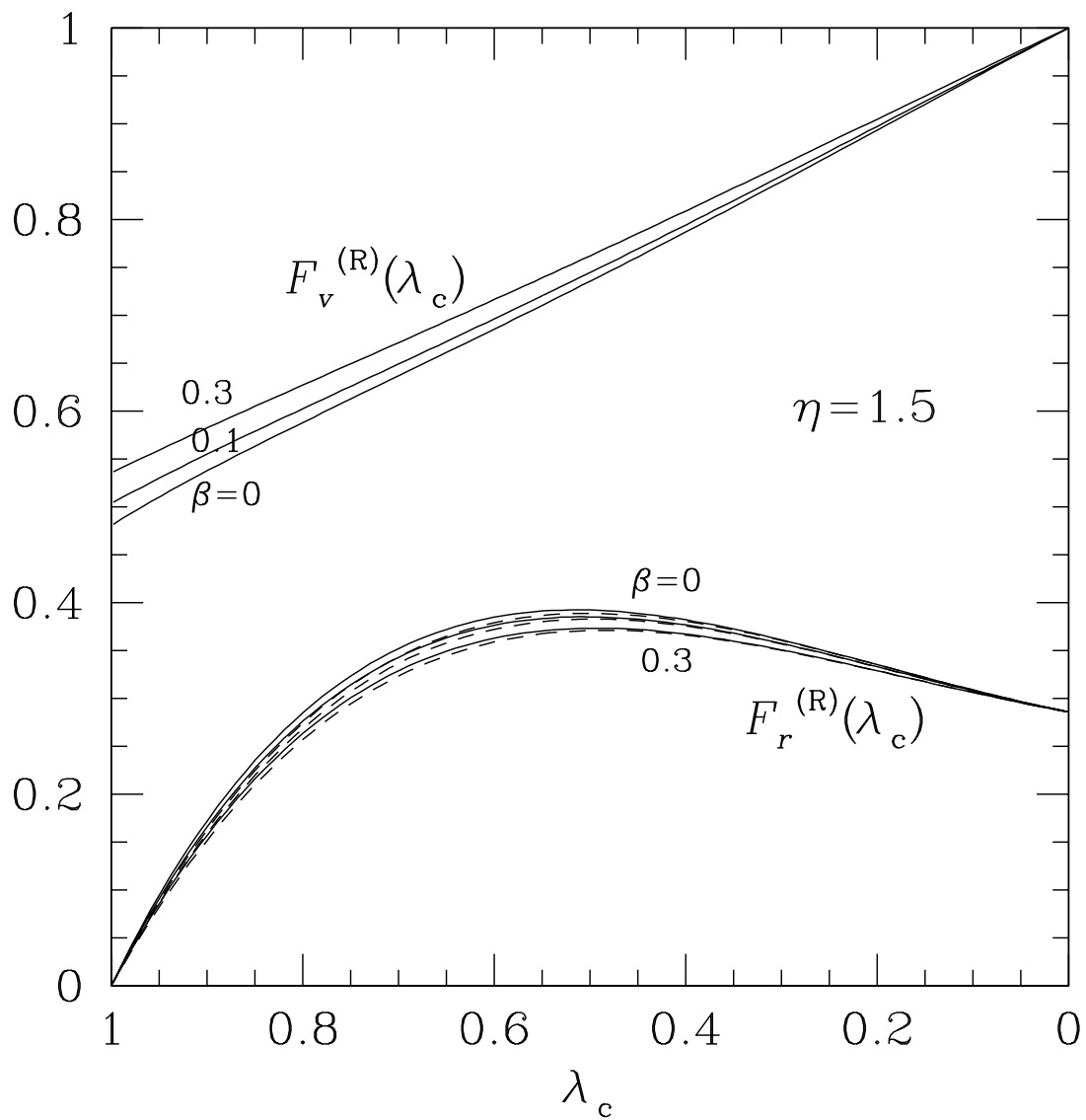


Fig. 4.— Plots of functions $F_v^{(R)}(\lambda_c)$ and $F_r^{(R)}(\lambda_c)$ for $\eta = 1.5$. The solid lines denote the accurate values of eqs.(27) and (30) and the dashed lines represent eq.(33). The solid and dashed curves of $F_r^{(R)}(\lambda_c)$ are plotted for $\beta = 0, 0.1$, and 0.3 , respectively, from upper to lower.

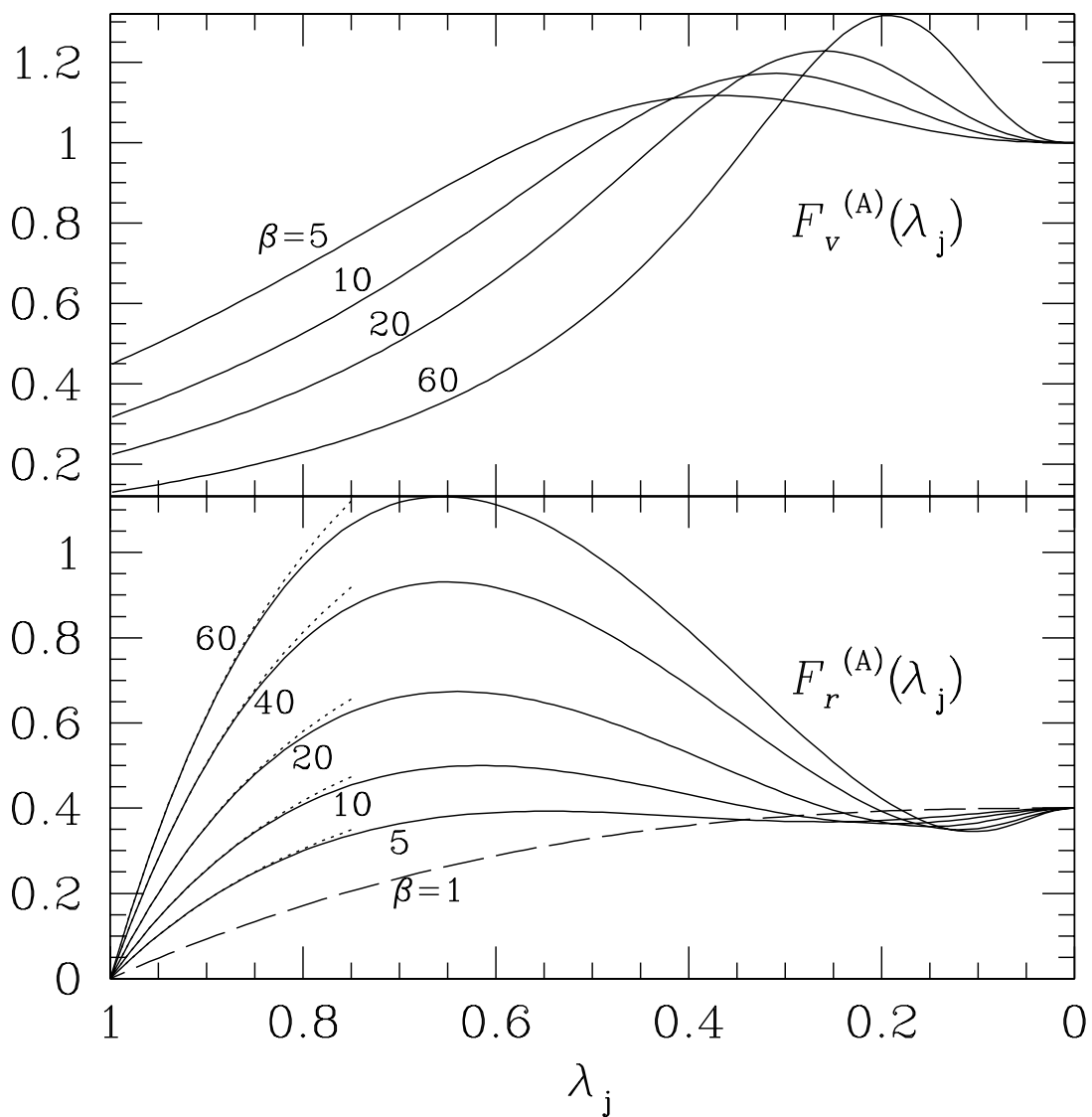


Fig. 5.— Plots of functions $F_v^{(R)}(\lambda_c)$ and $F_r^{(R)}(\lambda_c)$ for the breakout case ($\beta > 1$). The solid lines denote the accurate values of eqs.(8) and (11). The dotted lines represent the approximate series eq.(15). The long dashed line of $F_r^{(A)}$ for $\beta = 1$ is plotted merely for comparison.

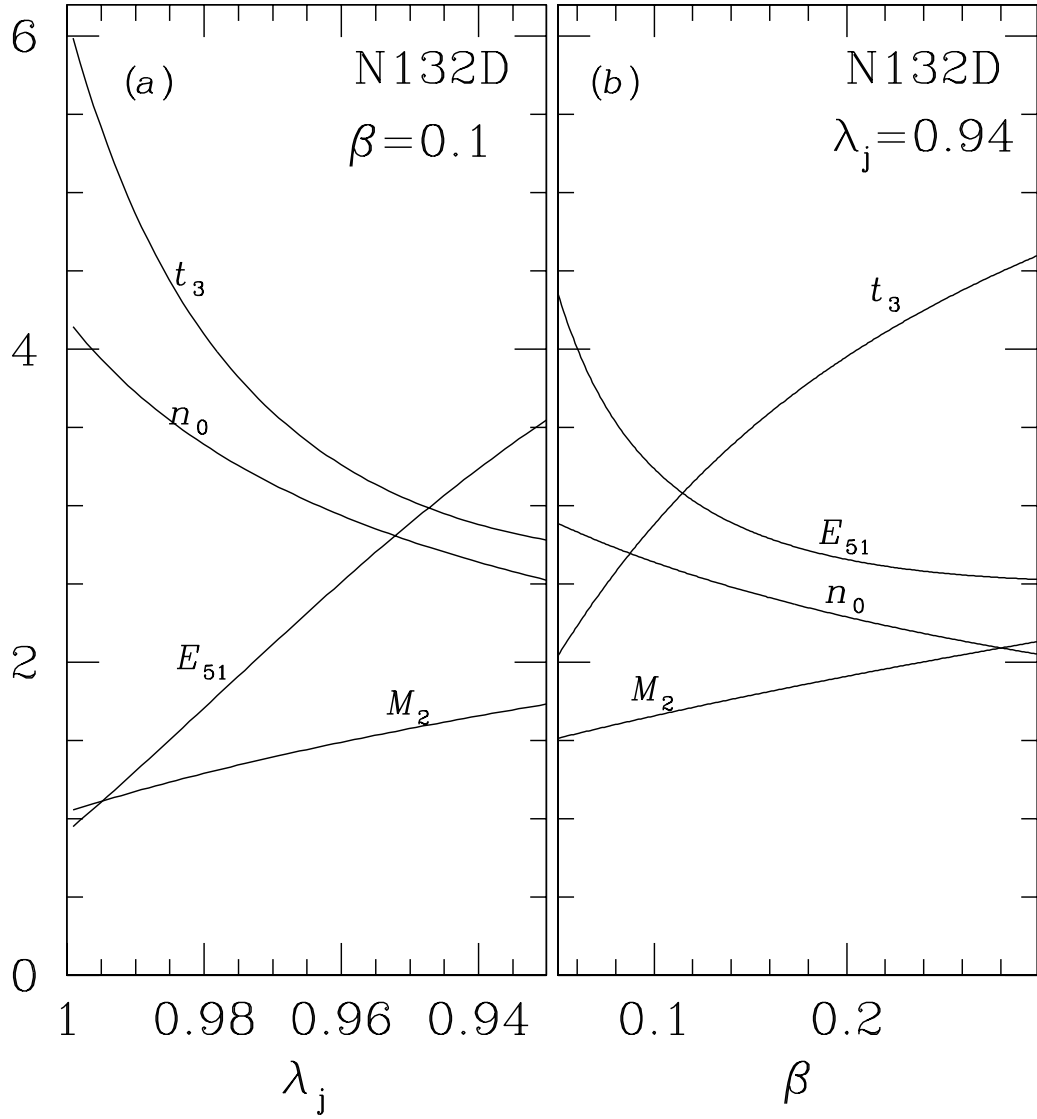


Fig. 6.— Plots of physical parameters derived for SNR N132D for $\beta = 0.1$ and $\lambda_j = 0.94$, respectively.